Building and Environment 222 (2022) 109442

Contents lists available at ScienceDirect

Building and Environment

journal homepage: www.elsevier.com/locate/buildenv

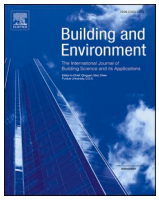

Energy performance of a prefabricated timber-based retrofit solution applied to a pilot building in Southern Europe

Gianpiero Evola [a,*], Vincenzo Costanzo [b], Alessandra Urso [b], Carola Tardo [b], Giuseppe Margani [b]

[a] Department of Electrical Electronic and Computer Engineering (DIEEI), University of Catania, Viale A. Doria 6, 95125, Catania, Italy
[b] Department of Civil Engineering and Architecture (DICAR), University of Catania, Via S. Sofia 64, 95125, Catania, Italy

ARTICLE INFO

Keywords:
Timber-based retrofit
Thermal insulation
Thermal bridges
Dynamic simulations
Space heating
Space cooling

ABSTRACT

This paper advances the current knowledge on the use of prefabricated timber-based panels in building renovation by analyzing in detail the thermal performance achieved by two different renovation solutions developed in the framework of the ongoing e-SAFE H2020 project. In particular, these solutions apply to the external walls of a pilot building located in Catania (Italy) as a double-skin façade that increases also the seismic performance of the building. The dynamic energy simulations reveal that the proposed solutions allow reducing the energy need for space heating and space cooling by 66% and 25%, respectively. One further finding is that, although the proposed timber-based renovation solutions are not affected by mould growth and surface condensation risk, the impact of thermal bridges cannot be neglected after renovation. Indeed, despite the strong reduction in the magnitude of heat losses due to thermal bridges (from 667 $W \cdot K^{-1}$ down to 213.1 $W \cdot K^{-1}$), they still account for about 21% of total heat losses after the renovation. This suggests that more complex and expensive technological solutions should be introduced to further reduce heat losses in some thermal bridges, but a cost-benefit analysis should justify their adoption. Finally, overlooking these thermal bridges in dynamic energy simulations can lead to an average underestimation of the heating and cooling energy demand after the renovation, by about 16% and 5% respectively. In this regard, the paper proposes a simplified yet reliable approach to include heat transfer through thermal bridges in the post-processing stage of dynamic energy simulations under thermostatic control.

1. Introduction

In Europe, buildings are responsible for 40% of the final energy consumption and for approximately 36% of greenhouse gas emissions [1], thus contributing to the climate change and the increase of related natural hazards (e.g. floods, hurricanes, storms, landslides, forest fires, desertification, melting of glaciers and sea level rise). The substantial energy demand of the existing building stock is mostly due to the poor thermal performance of their envelope components (e.g. roofs, walls and windows), and to the low efficiency of the heating and cooling systems. Both issues are especially evident in those buildings that were built when current EU regulations addressing energy efficiency in buildings were not in force: at present, it is possible to state that roughly 75% of the EU stock is energy inefficient. The energy renovation of this share of EU buildings can thus lead to significant savings, potentially reducing the EU's total energy demand by 5–6% and the carbon dioxide (CO_2) emissions by around 5% [2].

However, the enhancement of the energy efficiency of the existing building stock is not always enough to increase the sustainability level of our cities. Indeed, especially in earthquake-prone countries, which cover a relevant part of the European territory, renovation actions must include also structural safety [3]. The earthquakes occurred in Southern Europe in the last two decades (e.g. L'Aquila 2009, Italy; Emilia 2012, Italy; central Italy 2016; Durazzo 2019, Albania; Dodecanese 2020, Greece) demonstrated the high vulnerability of the building stock, as well as the catastrophic effects that buildings' damage or collapse can entail in terms of human losses and injuries, economic and social harm, and environmental impact [4]. However, the most common techniques to increase the seismic performance of the existing buildings are highly invasive, time-consuming, and very expensive [5], thus poorly accessible to the owners, especially to low-income families.

One of the main strategies for enhancing energy efficiency in existing buildings consists in increasing the thermal performance of the envelope components in order to reduce heat losses through surfaces and thermal bridges, for instance by adding further thermally insulating layers, while also avoiding indoor overheating in summer. In this case, renovation

* Corresponding author.
E-mail address: gevola@unict.it (G. Evola).

https://doi.org/10.1016/j.buildenv.2022.109442
Received 16 May 2022; Received in revised form 7 July 2022; Accepted 20 July 2022
Available online 31 July 2022

works might also be the chance to address and improve the seismic resistance. Indeed, several researchers have recently investigated novel retrofit solutions aimed at concurrently improving both the energy and seismic performance of the existing buildings. For instance, solutions based on the use of engineered steel exoskeletons [6–8] or wet-envelope technologies [9–11] have been recently proposed to renovate reinforced concrete (RC) framed buildings. These solutions primarily rely on the intervention from the outside, in order to minimize the occupant's disruption, and reduce demolition works, implementation time and costs.

However, the need for more sustainable approaches to building renovation has led the research community to investigate also other potential retrofitting materials than the traditional concrete and steel. Indeed, concrete and steel require high energy-intensive manufacturing processes that entail significant global carbon emissions [12].

In this regard, the use of wood and other engineered timber products like Cross Laminated Timber (CLT), together with wood-based insulating materials, showed great potential for retrofit purposes. Indeed, CLT has low density and thermal conductivity, meanwhile ensuring high stiffness, and thus combining structural and energy efficiency. Moreover, CLT stands out for its high level of prefabrication, is recyclable and provides high environmental sustainability. Different CLT applications have been recently investigated to upgrade the seismic and thermal performance of both the existing unreinforced masonry buildings and the RC framed ones. Nevertheless, the adoption of CLT as a retrofitting solution is still an open field of research and poses several technological challenges [13]. In this research context, Margani et al. [14] recently proposed an innovative integrated (seismic-energy and architectural) renovation solution, consisting in cladding the external envelope of RC framed buildings with structural and insulating prefabricated timber-based panels that are connected to the RC frame by means of innovative seismic energy dissipation devices. Compared with other more traditional retrofit solutions, this allows reducing the time needed for renovation works and the occupants' disruption. This technology, under development within the ongoing Horizon 2020 innovation project e-SAFE (Energy and Seismic AFfordable rEnovation solutions) [15], has been further developed and is now ready for being prototyped and tested in the renovation of a pilot building in Catania, (Southern Italy), which will be performed in 2023.

The aims of this paper are manifold. From a technological point of view, the paper aims at presenting the latest developments of the two renovation solutions introduced by e-SAFE – namely e-PANEL and e-CLT – and discusses the criteria that will guide their application to a pilot building in Southern Italy. Then, the paper aims at clarifying their effectiveness in improving the thermal performance of the pilot building, focusing on their ability to reduce heat losses through the building surfaces and through the thermal bridges, according to different scenarios in terms of insulation level. In this stage, thermal bridges are considered in detail through 2D numerical analysis leading to the definition of their linear thermal transmittance, their impact on the overall energy balance and the risk of condensation and mould formation.

Finally, the paper presents dynamic energy simulations at the building scale to assess the potential savings in space heating and cooling needs thanks to the proposed renovation solutions. To this aim, thermal bridges are included in the calculation of the energy needs through a dedicated post-processing of the hourly thermal loads, which proves to be a fast yet rigorous approach when simulations are performed under controlled indoor air temperature. This represents an advance in the current dynamic energy simulation modelling approach, for which it is common practice either to neglect or to oversimplify the influence of thermal bridges (e.g. by derating the U-value of the walls or by introducing fictitious surfaces with appropriate thermal resistance and no mass) because of the difficulties in easily dealing with them in dynamic simulation tools. The outcomes also suggest the extent of the error due to neglecting thermal bridges in dynamic simulations aimed at for estimating the energy demand in buildings.

2. Materials and methods

2.1. The renovation solution

The proposed retrofit technology consists in cladding the external envelope of an existing RC framed building with a new prefabricated timber-based shell that acts as a seismic-resistant and energy-efficient skin, while also contributing to renovating its architectural image (Fig. 1).

The seismic technology that drives this intervention relies on the use of structural CLT-based panels (called e-CLT) applied to the outer blind walls, by connecting them to the RC beams through innovative seismic energy dissipation devices. These devices are friction dampers consisting in two steel profiles, which connect the CLT panels of two consecutive storeys [16]. The intervention aims at increasing both the seismic and dissipative capacity of the RC structure, by exploiting the high mechanical properties of CLT and the additional energy dissipation source, respectively. The effect of these multiple features could reduce the storey drifts demanded by the earthquake to values compatible with the structure capacity, thus preventing its collapse.

The e-CLT panels are combined with non-structural panels (called e-PANEL) that are placed on the outer windowed walls. The e-PANEL includes new high-performing windows (multiple glazing with low-emission coating, wooden frames, etc.) that replace the existing ones. Since the e-PANEL has no structural strengthening role, it has a lightweight wooden frame to ensure easier manufacture, low environmental impact, and cost savings. Furthermore, it is not equipped with friction dampers, but it connects to the existing RC beams through steel brackets and anchors with appropriate seismic resistance. Overall, the distribution of e-CLTs and e-PANELs also depends on the seismic vulnerability of the building, the seismicity of the specific area, as well as the expected level of seismic upgrading.

Finally, e-CLTs and e-PANELs also provide thermal and sound insulation, since they integrate insulating and resilient materials to increase the thermal resistance of the existing walls and reduce the noise transfer to the internal spaces. Both panels are conceived to be prefabricated off-site and to be installed from the outside of the building through mobile lifting equipment (cranes, lifting platforms, etc.), thus avoiding the disruption of traditional scaffoldings and the occupant's relocation during works.

Each panel thus integrates: i) a layer of thermal-acoustic insulation material; ii) a weatherproof vapour-open membrane; iii) the finishing layer (Fig. 2). The insulation material can be chosen according to the local availability of low-cost bio-materials (e.g. wood fibre, hemp, cork, cellulose fibre, etc.), and its thickness is set to achieve values of thermal transmittance that comply with national regulations. The membrane protects the main layers of each panel (i.e. insulation materials, CLT panel etc.) from rainwater and reduces condensation issues. Then, the finishing layer (e.g. wood plastic composite, ceramic, stone, porcelain stoneware, glass, rendered fiber boards, wood, etc.) can be chosen according to the users' aesthetic preferences and may be separated from the other layers by a ventilated air cavity to reduce building thermal loads in summer, while also drying possible rainwater infiltration or winter moisture.

The e-PANEL also requires an air cavity between the cladding and the insulation layers to match the overall e-CLT thickness (Fig. 2). Moreover, the window integrated into the e-PANEL can be equipped with external sun shading systems (e.g. venetian blinds, roller shutter etc.) to reduce indoor overheating in summer, thus increasing the indoor thermal comfort.

The proposed retrofit solution also provides the use of further prefabricated panels that cover the dampers after the e-CLT and e-PANEL installation, while also allowing easy inspection and maintenance (Fig. 3). These components integrate thermal insulation materials to reduce the thermal bridges at the beams level and are cladded off-site or on-site to ensure aesthetic uniformity on the building façade.

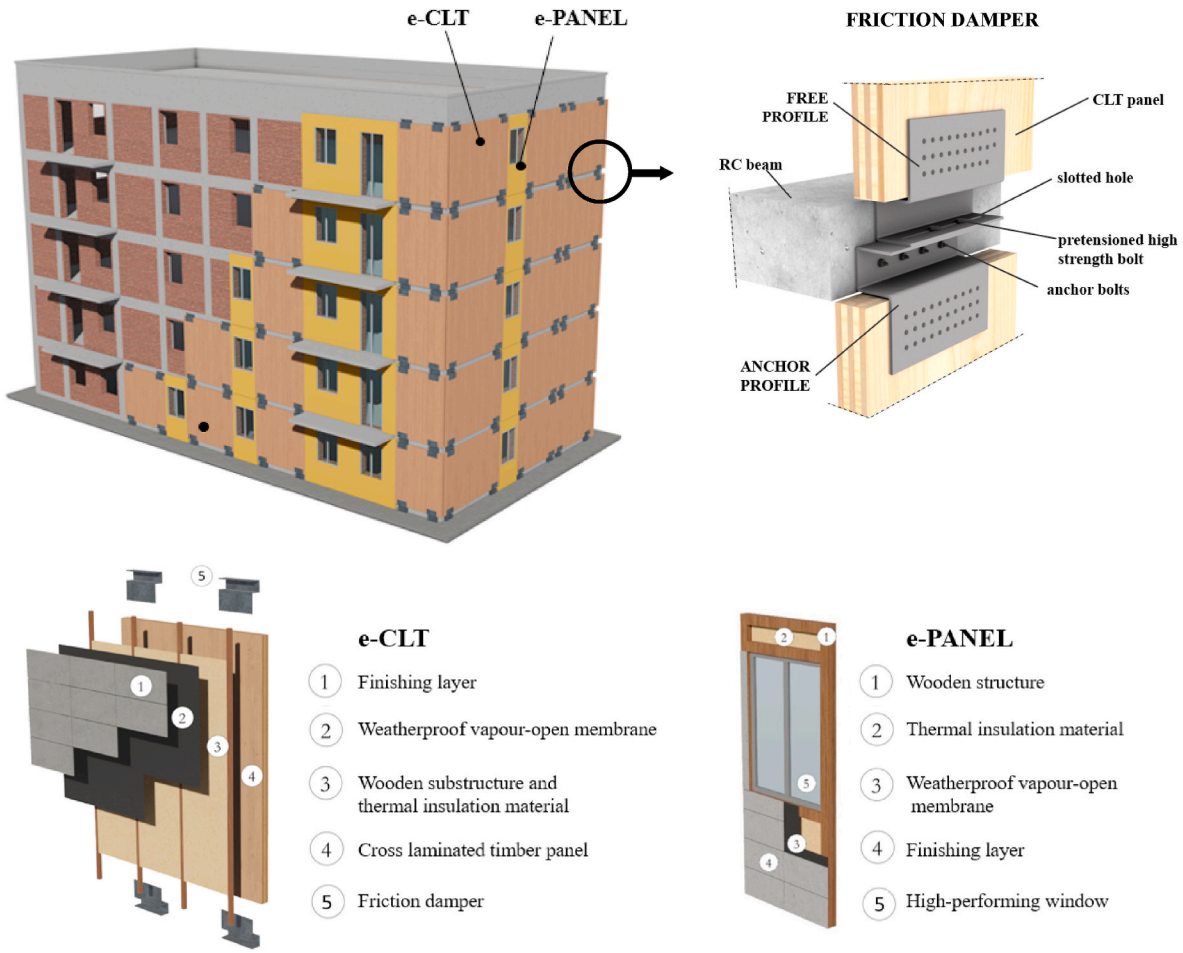

Fig. 1. Components of the proposed e-SAFE retrofit technologies.

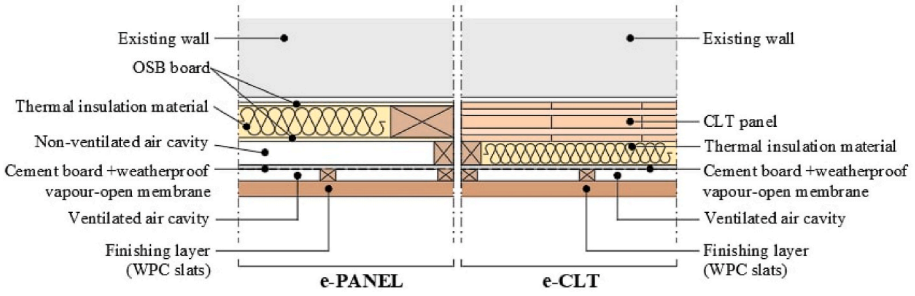

Fig. 2. Horizontal section of e-CLT and e-PANEL.

The proposed technology can be also combined with roof thermal insulation interventions, especially if national regulations call for them. Indeed, it is highly advisable to involve the entire building envelope when approaching the energy retrofit of an existing building.

2.2. The pilot building

The pilot building is a RC framed apartment block (Fig. 4) built in 1964 and located in Via Acquicella Porto, in the city of Catania (Lat: 37.30 North, Long: 15.07 East), which is characterized by warm and humid summer and moderately cold and wet winter seasons. According to the Köppen-Geiger climate classification, it is a typical example of Mediterranean climate (Csa climate type, [17]).

The pilot building belongs to a compound owned by the local public housing authority IACP Catania (Istituto Autonomo Case Popolari). The pilot building has five stories with two residential units for each one, and a roughly rectangular footprint whose gross size is 24 × 9.5 m. Each apartment has a net floor area of 94 m^2, while the net height is 2.85 m, resulting in an overall net heated volume V = 2680 m^3 for the entire building. The overall window surface is 144.2 m^2. The surface-to-volume ratio, i.e. the ratio of the gross dispersing surface to the gross heated volume, is 0.47.

At current state, the external infill walls are made of two leaves of hollow light concrete blocks (8-cm thick internal leaf and 12-cm thick external one), made of cement and light volcanic aggregates, with an intermediate non-ventilated, non-insulated air cavity (9-cm thick). Since there is no information about the stratigraphy of the slabs, the ground floor, the intermediate slabs and the roof have been assumed made of RC

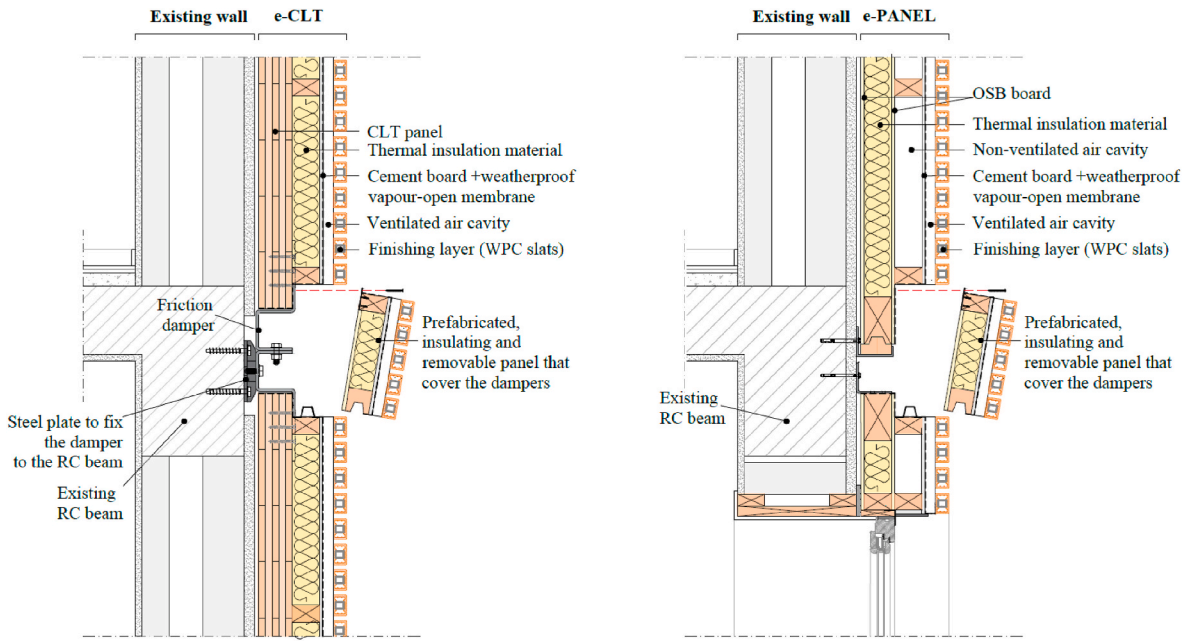

Fig. 3. Vertical section of the e-CLT and e-PANEL solutions.

Fig. 4. The pilot building in its current state.

and hollow clay blocks (20-cm thick) without thermal insulation, according to the construction techniques used in Southern Italy in the 1960s. The roof is flat with tiles flooring laid over a cement screed. The windows have single glazing ($g = 0.85$, $\varepsilon = 0.87$) with a metallic frame and no thermal break.

Table 1 and Table 2 summarize the assemblies' description and their thermal properties, while Table 3 resumes the U-values of all the envelope components, calculated by including the internal ($R_{si} = 0.13$ m^2 K·W^{-1}) and external ($R_{se} = 0.04$ m^2 K·W^{-1}) surface thermal resistance, according to EN ISO Standard 6946 [18]. The albedo of the outer surfaces is set as 0.4.

As far as the ground floor slab is concerned, it shows the same features as any other intermediate slab in the building, but it is on top of an underground non-heated space, whose height is 2.10 m and whose floor consists in a 10-cm thick cement screed lying on a 40 cm thick crawl space. The equivalent U-value of the ground floor slab, which also accounts for the heat transfer from the unheated space to the ground according to EN ISO Standard 6946 [18], is 0.64 W•m^{-2} K^{-1}: this value is half the U-value of the slab itself (see Table 3).

Just few apartments have some old and inefficient split units, mainly used for cooling purposes, while space heating is performed through portable gas stoves. However, in the following analysis the above real thermal systems are neglected, since the paper addresses the energy performance of the building envelope only.

According to the concept of the proposed retrofit system, in the renovation stage the structural e-CLT panels overlap the outer blind walls of the pilot building, with a uniform distribution on the opposite building fronts, while the e-PANELs apply to all the windowed walls (Fig. 5). Based on the criteria used for the panel's application, e-CLTs and e-PANELs occupy an area of 757 m^2 and 231 m^2, respectively.

The e-CLT panels include a 10-cm thick CLT plate, while different insulation scenarios have been analysed for both e-CLT and e-PANEL, as better described in Section 3.1. Within the scope of this paper, the different ratio between the area of the insulation material and the interposed wooden frame compared to the total surface of both panels is here reported. Specifically, in the e-PANEL the wooden frame occupies here an area equal to about 50% of the total opaque panel surface, while

Table 1
Wall assembly for the pilot building: outside walls.

Material	s [mm]	λ [W•m^{-1}•K^{-1}]	R [m^2•K·W^{-1}]	ρ [kg•m^{-3}]	c [J•kg^{-1}•K^{-1}]
Gypsum plaster	20	0.57 [19]	0.035	1300	1000
Hollow light concrete blocks	80	0.29 [20]	0.276	845	1000
Non-ventilated air cavity	100	–	0.180	1.3	1000
Hollow light concrete blocks	120	0.39 [20]	0.307	667	1000
Cement plaster	30	0.9 [19]	0.033	1800	1000

Table 2
Floor assembly for the pilot building: intermediate slab.

Material	s [mm]	λ [W•m^{-1}•K^{-1}]	R [m^2•K•W^{-1}]	ρ [kg•m^{-3}]	c [J•kg^{-1}•K^{-1}]
Floor tiles	10	1.47 [19]	0.007	1500	1000
Cement mortar	10	1.40 [19]	0.007	2000	1000
Cement screed [a]	40	0.58 [19]	0.007	1400	1000
RC and hollow clay blocks	20	–	0.310 [21]	1130	840
Cement plaster	20	0.57 [19]	0.035	1300	1000

[a] In the roof slab, this layer has a higher thickness (on average 140 mm).

Table 3
U-values for the envelope components of the pilot building.

Building component	U-value
External infill wall	1.0 W•m^{-2} K^{-1}
Intermediate floor slabs	1.3 W•m^{-2} K^{-1}
Attic floor slab	1.2 W•m^{-2} K^{-1}
Windows	5.9 W•m^{-2} K^{-1}
Box for windows shutters	6.0 W•m^{-2} K^{-1}

the area of the insulation material corresponds to the other 50%. Instead, in the e-CLT the wooden frame interposed to the insulation material occupies only less than 10% of the total panel surface, which makes it negligible.

A cladding layer made of wood-plastic composite (WPC) slats has been assumed for both kinds of panels. Fig. 6 shows the potential architectural image of the considered building after the proposed renovation solution.

2.3. Thermal bridges

Thermal bridges are those parts of the building envelope where thermal resistance is modified either by a local change in the geometry of the structures or by a partial penetration of the building envelope by materials with different thermal conductivity [22]. They contribute in a non-negligible way to the heat losses through the building envelope, and this is most evident in buildings with RC frames. Indeed, the thermal conductivity of reinforced concrete usually ranges between 2 W•m^{-1} K^{-1} and 2.5 W•m^{-1} K^{-1}, while other building materials (e.g. cement screed, lightweight concrete, clay bricks) have much lower thermal conductivity ($\lambda \leq 1$ W•m^{-1} K^{-1}). For this reason, the presence of RC beams, pillars and balconies locally increase heat transfer and implies local "cold points", where mould formation can occur.

Fig. 7 classifies the typologies of thermal bridges identified in the pilot building and that will be included in the calculation of the heat losses.

To quantify the heat losses through a thermal bridge, it is common practice to attribute a linear thermal transmittance Ψ, which can then be multiplied by the length of the thermal bridge and by the indoor-outdoor temperature difference, as in Eq. (1):

$$Q_{TB} = \psi \cdot L \cdot (T_{in} - T_{out}) \quad (1)$$

The linear thermal transmittance of a thermal bridge can be determined from atlases compliant with the recently updated UNI EN ISO 14683:2018 [23,24], but these usually refer to generic configurations. Otherwise, a much more reliable approach consists in performing a finite element analysis by means of numerical software tools. According to the procedure set by the Standard EN ISO 10211 [22], a 2D finite element analysis implies that the thermal bridge has unit size along the

Fig. 6. Potential rendering of the pilot building after its renovation.

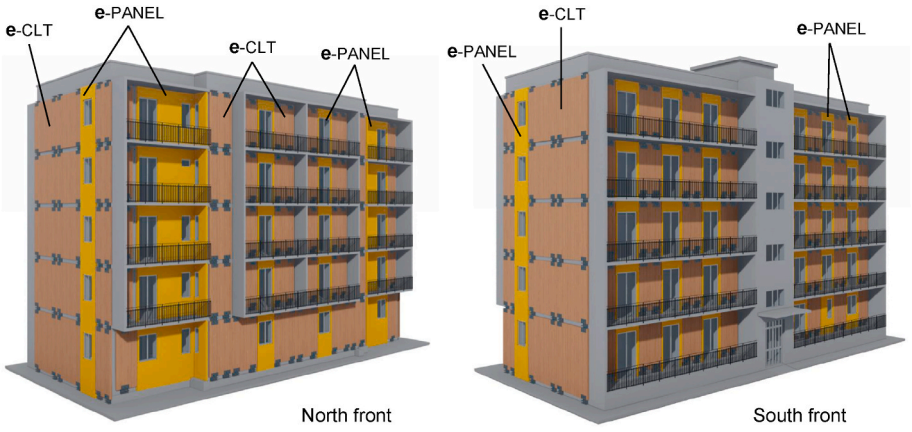

Fig. 5. The proposed distribution of e-PANEL (yellow surfaces) and e-CLT (brown surfaces), according to the criteria set in this research (e-CLTs and e-PANELs are reported without insulation and cladding layers). (For interpretation of the references to colour in this figure legend, the reader is referred to the Web version of this article).

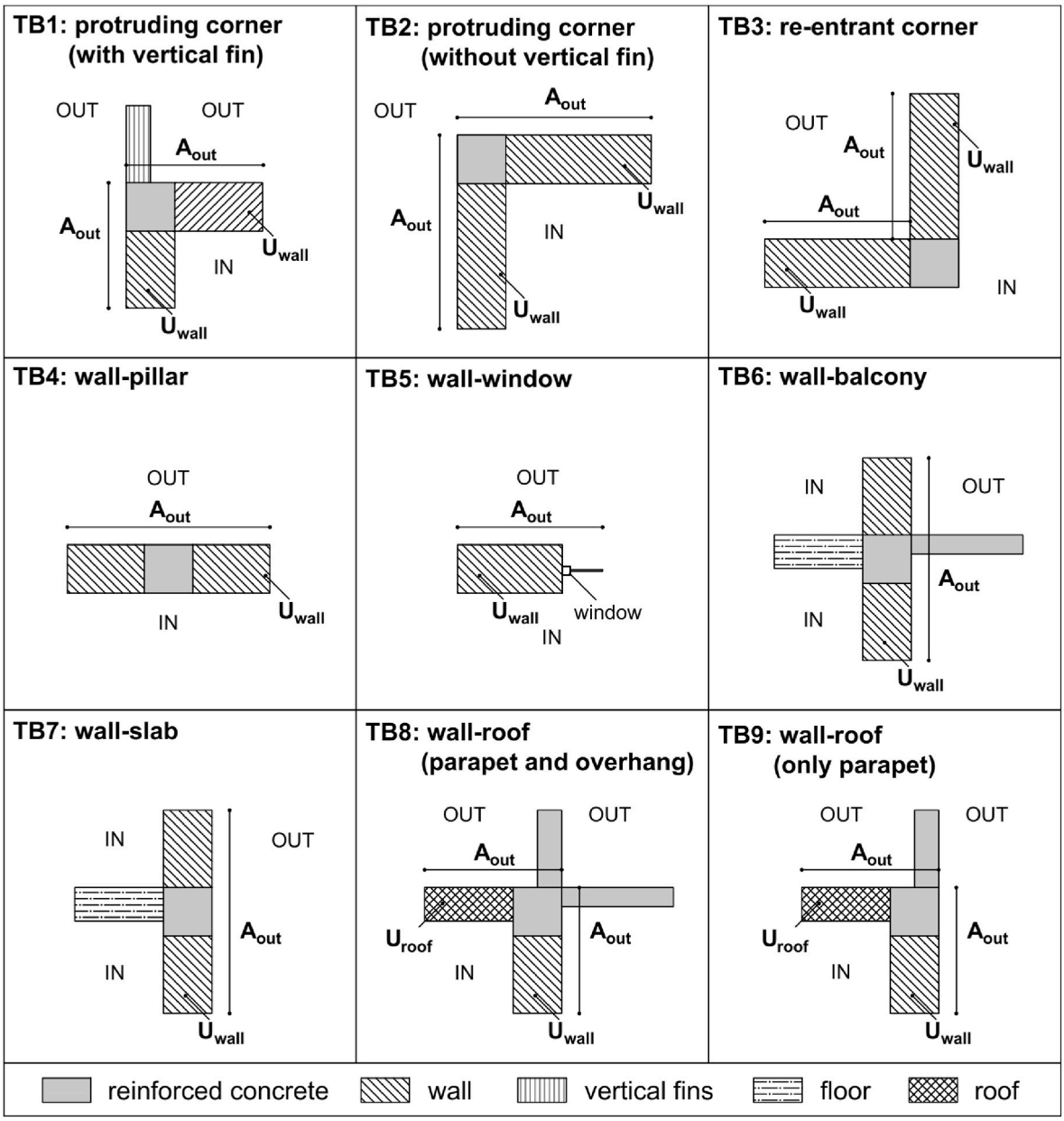

Fig. 7. Typologies of thermal bridges identified in the pilot building.

third dimension: as a result, it provides the total thermal power transferred through the element (Q_{TOT}) per unit length. Then, by means of Eq. (2) and Eq. (3), one can calculate the thermal coupling coefficient L_{2D} (in $W \bullet m^{-1} \bullet K^{-1}$) and the linear thermal transmittance, respectively, the latter by subtracting the thermal power transferred through the envelope surfaces under one-dimensional heat flux conditions.

$$L_{2D} = \frac{Q_{TOT}}{(T_{in} - T_{out})} \tag{2}$$

$$\psi_{out} = L_{2D} - \sum_{j} (U_j \cdot A_{out,j}) \tag{3}$$

A further result obtained through the 2D numerical simulations is the temperature field inside the building component, which allows identifying the minimum indoor surface temperature and thus understanding if risks of condensation or mould growth occur. It is here useful to remind that condensation occurs when the indoor surface temperature gets below the dew-point temperature associated with the indoor conditions, while mould is likely to grow when the relative humidity assessed at the surface temperature, and with the same vapour content as in the indoor air, is at least RH = 80% [25].

In this paper, this approach applies to all thermal bridges listed in Fig. 7: here, the outer size of the components per unit length (A_{out}) is also identified. The 2D finite element analysis is performed in steady state conditions and with isotropic materials through the software tool IRIS 5.0 [26], under the following assumptions:

- thermal conductivity of reinforced concrete: $\lambda = 2.5\ W \bullet m^{-1}\ K^{-1}$
- indoor and outdoor temperatures: $T_{in} = 20\ ^{\circ}C$ and $T_{out} = 5\ ^{\circ}C$
- indoor and outdoor relative humidity: $RH_{in} = 65\%$ and $RH_{out} = 85\%$

The outdoor conditions correspond to the average monthly weather conditions in the colder months in Catania, while the indoor conditions are those used for hygrothermal simulations according to the national regulations [27,28]. Fig. 8 reports three examples of the thermal bridges simulated in IRIS. In order to simplify the 2D model, the metal dampers

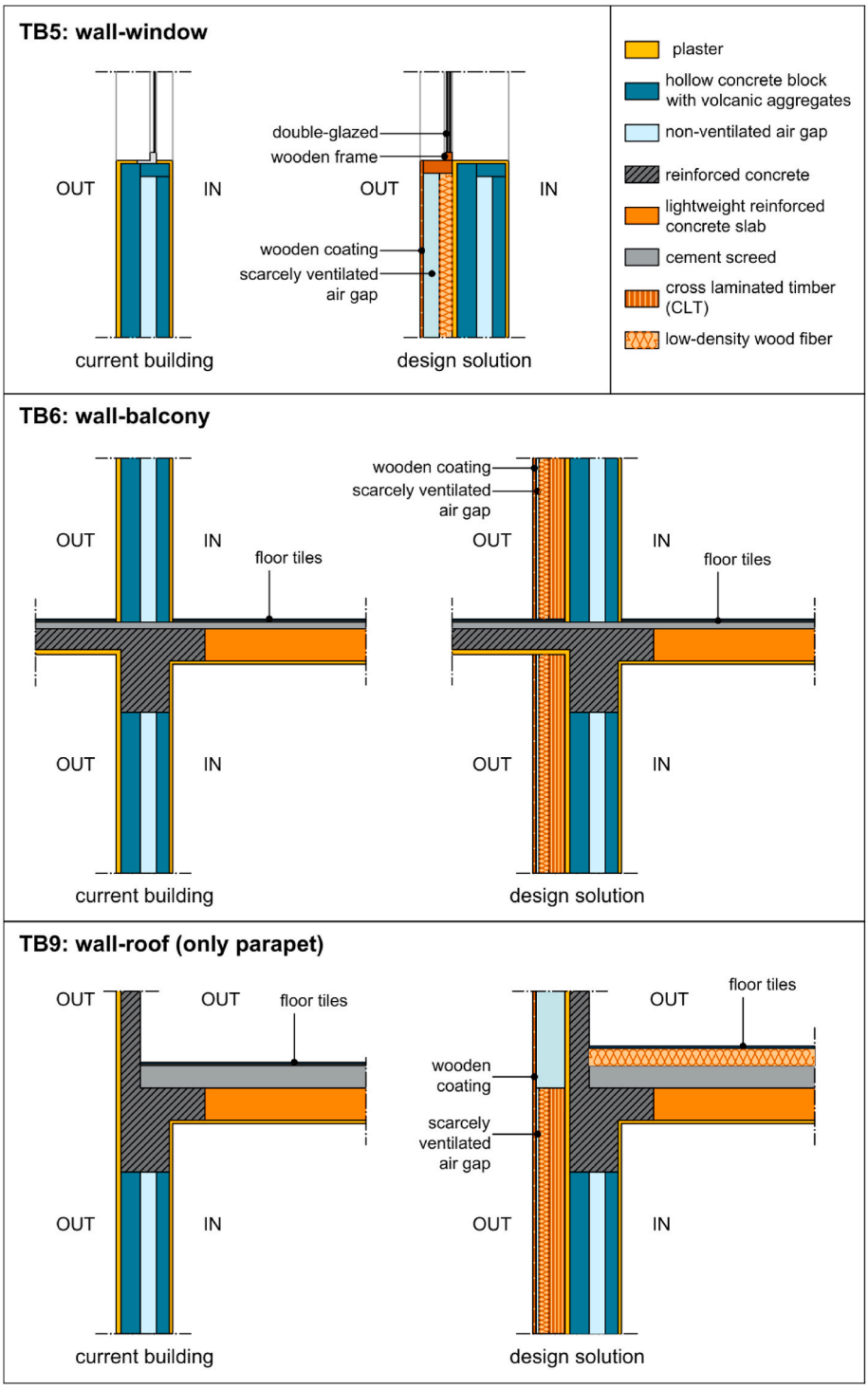

Fig. 8. Detailed stratigraphy used in IRIS to assess thermal bridging effect.

that connect the CLT boards to the RC beams are not included in the figures; however, the finite element analyses also included them in order to verify their impact on the overall energy balance of the renovated building.

Finally, by accounting for all thermal bridges identified in Fig. 7, each one having its overall length in the pilot building, it is possible to calculate the heat loss coefficient H_{TB} (in $W \cdot K^{-1}$): in Eq. (4), $nt = 8$ in this case. The entire building can also be described through an overall heat loss coefficient per unit surface (H'): it is assessed as in Eq. (5), where *ns* is the total number of dispersing surfaces in the building envelope. This parameter is particularly relevant since it is recalled by Italian regulations.

$$H_{TB} = \sum_{j=1}^{nt} \psi_{out,j} \cdot L_j \tag{4}$$

$$H' = \left(\sum_{k=1}^{ns} U_k \cdot A_{k,out} + H_{TB} \right) \Big/ \left(\sum_{k=1}^{ns} A_k \right) \tag{5}$$

2.4. Settings for dynamic energy simulations

The dynamic energy simulations of the pilot building are run on an hourly basis through the largely validated EnergyPlus v.9.0.1 software tool [29]. Fig. 9 shows the typical plan of the pilot building; each floor hosts two apartments according to a common internal layout, with a stairwell in the Southern front. The figure also identifies the thermal zones adopted for simulation purposes, and the resulting 3D model built in SketchUp through the Open Studio plug-in. Parapets, balconies and vertical fins are included in the model just as opaque shading components, meaning that no specific material is set.

Some modelling assumptions introduced in the simulations are worth discussing, since they may affect the outcomes of the simulations.

First, heat transfer through the non-ventilated underfloor zone is simulated by means of the Other Side Coefficient function: in this case, the same weighting factor (50%) is attributed to the indoor air temperature and the outdoor air temperature, coherently with the equivalent U-value determined in Section 2.2.

Then, the incoming outdoor airflow rate is defined through a fixed hourly value amounting to 0.5 h^{-1} (average intentional ventilation rate) plus an additional contribution related to adventitious infiltrations, which accounts for the specific building location, the number of floors and the surrounding building density. The air infiltration rate is determined based on the *Effective Leakage Area* (ELA) method proposed by the ASHRAE Handbook [30]. This approach dynamically considers both stack and wind effects once a *leakage area* A_L (cm^2) is set for every thermal zone in the building, based on Eq. (6):

$$A_L = \frac{n_{50} \cdot V}{3600} \cdot \sqrt{\frac{\rho}{2 \cdot \Delta p_{50}}} \cdot 1000 \tag{6}$$

here, n_{50} is the air change rate at a pressure difference $\Delta p_{50} = 50$ Pa: the paper assumes $n_{50} = 8\ h^{-1}$, which is the value suggested by the UNI 11300/1:2014 Standard [31] for envelopes with high permeability, while $\rho = 1.2\ kg/m^3$ is the standard air density. The resulting values for every thermal zone of the typical apartment are summarized in Table 4.

Once A_L is set, the air infiltration rate expressed is eventually determined through Eq. (7):

$$Q_{inf} = \frac{A_L}{1000} \cdot \sqrt{C_S \cdot (T_{in} - T_{out}) + C_W \cdot w^2} \tag{7}$$

The values used for the stack coefficient ($C_S = 4.35 \bullet 10^{-4}\ L^2\ s^{-2}\ cm^{-4} \bullet K^{-1}$) and the wind coefficient ($C_W = 2.71 \bullet 10^{-4}\ L^2\ cm^{-4}\ m^{-2}$) are retrieved in the ASHRAE Handbook, and depend on the number of floors and the surrounding buildings density.

Further input data for the energy simulations are the occupancy profiles, the interior lighting and the electric equipment, whose maximum values are reported in Table 5. These internal gains depend on the specific hourly occupancy and room function: in particular, the kitchen is occupied during lunch hours, the living room from 7 p.m. to 11 p.m. and the bedrooms from 11 p.m. to 7 a.m., respectively. Finally, the heating and cooling set point temperatures are 20 °C and 26 °C respectively, while their schedule is reported in Table 5.

The results of simulations eventually consist in a series of hourly values for the heating/cooling demand of an ideal all-air system that is always able to meet the thermal load of each thermal zone. Then, the seasonal energy demand results from integrating the hourly values over the heating/cooling periods reported in Table 5, and by referring the result to the unit net surface of the building.

The weather file used to run the simulations is a Typical Weather Year (TWY) developed by the same authors, based on weather data recorded from 2002 to 2019 by a weather station located just 7 km far from the pilot building. The procedure used to develop the TWY is described in a previous paper [32] and follows the IWEC format defined by ASHRAE [33,34].

One further innovative methodological aspect of this work is the way thermal bridges are managed in the dynamic simulations. Indeed, EnergyPlus does not allow including thermal bridges with their linear thermal transmittance while characterizing the building envelope: some researchers have overcome this limitation by adding fictitious surfaces in the SketchUp geometric building model, and appointing them an equivalent thermal transmittance that includes the linear thermal transmittance [35]. However, this approach complicates the preparation of the geometric model for simulation purposes, and means also changing the properties of the wall layers. Instead, in this paper the contribution of thermal bridges to the heating/cooling load has been included through post-processing operations by adding, on hourly basis and throughout the year, the result of Eq. (8) to the thermal load provided by simulating the building without thermal bridges:

$$Q_{TB} = H_{TB} \cdot (T_{in} - T_{out}) \tag{8}$$

Here, H_{TB} has been preliminary calculated as in Eq. (4), the outdoor temperatures are available in the weather file and the indoor temperatures are those reported as an output by EnergyPlus. The proposed approach for including the heat transfer through thermal bridges in the dynamic simulations is fully reliable as long as the indoor temperatures are set to a constant value: this is the case of an ideal all-air system acting under thermostat conditions. On the other hand, in free-running simulations – where the indoor temperature evolves with time according to the thermal loads – it cannot be useful.

3. Results and discussion

3.1. Thermal features of the proposed envelope solutions

In a first stage, three different insulation scenarios are considered for the external walls of the pilot building:

Fig. 9. 3D model of the pilot building in SketchUp, and corresponding internal layout.

Table 4
Effective leakage area for every thermal zone equipped with windows.

Thermal zone	Bedroom 1	Bedroom 2	Bedroom 3	Kitchen	Laundry	Living room	WC
A_L [cm^2]	128.6	91.2	127.4	60.7	24.5	107.0	39.9

Table 5
Internal gains and buildings' operational schedules.

Lighting and equipment	4 W•m^{-2} during people occupancy
People occupancy	0.04 person/m^2, suitable hourly profiles (sedentary activities, 100 W/person)
Heating system (20 °C)	From December 1st to March 31st every day (6 a.m.–8 a.m., 5 p.m.–11 p.m.)
Cooling system (26 °C)	From June 1st to September 30th every day (9 a.m.–9 p.m.)

- Low insulation scenario: 40 mm (e-CLT) and 60 mm (e-PANEL)
- Basic insulation scenario: 60 mm (e-CLT) and 80 mm (e-PANEL)
- Enhanced insulation scenario: 80 mm (e-CLT) and 120 mm (e-PANEL)

The thickness of the insulating material (low-density wood fiber) applied to the e-CLT and the e-PANEL is not the same: both values are commercially available, and are selected in order to ensure similar U-values for the two panels, thus a certain uniformity in the thermal insulation level of all opaque vertical facades. Table 6 reports the thermal properties of the layers added to the existing walls in the renovation stage. Of course, the CLT layer does not apply to the e-PANEL: since the two kinds of panels must have the same overall thickness, in the e-PANEL the air gap increases, but its thermal resistance does not change. Indeed, according to EN ISO Standard 6946 [18], the thermal resistance of vertical air gaps keeps constant above 18 mm of thickness. It is also worth reminding that in this case the air gap can be configured as "scarcely ventilated", which allows halving the thermal resistance value applied to non-ventilated gaps.

Now, the U-value of the portions of renovated walls where e-CLT applies can be calculated as in Eq. (9):

$$U_{CLT} = \left(R_{wall} + \frac{s_{CLT}}{\lambda_{CLT}} + \frac{s_{ins\_CLT}}{\lambda_{ins}} + R_{GAP} \right)^{-1} \quad (9)$$

Instead, such a direct calculation is not possible for the e-PANEL, where in a considerable portion of the overall opaque surface (in this pilot amounting to around 50%) the wooden studs interrupt the insulating material (see Fig. 2). Actually, in the e-PANEL the heat flux cannot be regarded as mono-dimensional, and this deserves a more detailed investigation. To this aim, the e-PANEL has been modeled through the same finite element tool used for the thermal bridges, which provided the average U-value reported in Table 7.

Table 6
Layers of materials included in the e-CLT solution.

Material	s [mm]	λ [W•m^{-1}•K^{-1}]	ρ [kg•m^{-3}]	c [J•kg^{-1}•K^{-1}]
Existing wall	350	Thermal resistance: R_{wall} = 1.00 m^2 K·W^{-1}		
Cross Laminated Timber (CLT)	100[a]	0.130	438	1600
Insulation (low-density wood fiber)	[b]scenario	0.038	50	2100
Scarcely ventilated air gap	20[a]	Thermal resistance: R_{GAP} = 0.09 m^2 K·W^{-1}		
WPC slats	30	Negligible thermal resistance		

[a] No CLT applies to the e-PANEL, so the air gap increases.
[b] According to the scenario considered in the calculation.

Table 7
U-values for the vertical opaque surfaces after renovation with e-CLT and e-PANEL.

Envelope solution	Insulation scenario		
	Low	Basic	Enhanced
e-CLT	0.343 W•m^{-2} K^{-1}	0.291 W•m^{-2} K^{-1}	0.252 W•m^{-2} K^{-1}
e-PANEL	0.431 W•m^{-2} K^{-1}	0.370 W•m^{-2} K^{-1}	0.320 W•m^{-2} K^{-1}
Entire vertical opaque envelope (Eq. (10))	0.362 W•m^{-2} K^{-1}	0.307 W•m^{-2} K^{-1}	0.267 W•m^{-2} K^{-1}

Finally, the average U-value for the entire vertical opaque envelope (including e-CLT and e-PANEL) is determined as:

$$U_{avg\_op} = \frac{A_{CLT} \cdot U_{CLT} + A_{PANEL} \cdot U_{avg\_PANEL}}{A_{CLT} + A_{PANEL}} \quad (10)$$

This value is very useful for the sake of comparison with the requirements of national regulations. For instance, the Italian regulation concerning major renovations [28] states that, in climate zone B, the average thermal transmittance for the entire opaque vertical envelope must not exceed 0.40 W•m^{-2} K^{-1}, which is ensured even by the "low insulation" scenario (U = 0362 W•m^{-2} K^{-1}). However, climate zone B is representative of a very low number of municipalities in Italy, while the rest of the Country falls in colder climate zones with lower U-value thresholds. Furthermore, the U-value attained by the "low insulation" scenario would not comply with the great majority of European national laws (except in Greece, Cyprus, Spain and Turkey) [36]. For this reason, the adoption of the "basic insulation" scenario – implying just 2 cm more insulation – is a better option, which also cuts the average U-value by 20%.

Finally, the current windows are replaced with low-e double glazing windows with wooden frame (U = 1.8 W•m^{-2} K^{-1}). The retrofit solution also envisages the possibility of insulating the attic floor slab through 10 cm of high-density wooden fibre (λ = 0.035 W•m^{-1} K^{-1}), meaning a final U = 0.27 W•m^{-2} K^{-1} for the roof floor in the renovated building. Instead, applying a thermal insulation layer in the ground floor slab is not technically easy, since this would generally imply high disruption for the residents (in particular for furniture removal, flooring demolition, door cutting, etc.): however, the simulations will also investigate this opportunity (with 4 cm of insulation) in order to quantify the potential benefits. The albedo of the outer surfaces is kept at 0.4, as in the current state.

3.2. Heat losses and condensation issues in thermal bridges

The heat losses due to thermal bridges are here studied in relation to the current building configuration and after the building renovation. In the second case, "basic insulation" of the external walls is considered, including the insulation of the roof. The results are reported in Table 8 and Fig. 10, and do not include the effect of the metal dampers that connect the e-CLT to the beams: however, further discussion on their role is included at the end of this Section.

First, it is interesting to underline that the thermal bridges showing the highest heat loss per unit length in the current building are, in order, TB6 (connection between walls and balconies), TB7 (connection between walls and slabs) and TB4 (connection between pillar and wall), as reported in Table 8. This confirms that wall-to-floor thermal bridges are

Table 8
Linear thermal transmittance of thermal bridges: comparison between the current building and its renovated version.

Code	Type of thermal bridge	L	Current building		After retrofit	
			Ψ_{out}	H_{TB}	Ψ_{out}	H_{TB}
		[m]	[W·m^{-1}·K^{-1}]	[W·K^{-1}]	[W·m^{-1}·K^{-1}]	[W·K^{-1}]
TB1	Protruding corner (with fin) pillar	50.8	−0.030	−1.5	0.019	1.0
TB2	Protruding corner (without fin)	33.8	−0.029	−1.0	−0.085	−2.9
TB3	Re-entrant corner with pillar	28.2	0.497	14.0	0.062	1.7
TB4	Outside wall – pillar	126.9	0.834	105.8	0.042	5.3
TB5	Outside wall – window	462.4	0.392	181.3	0.096	44.4
TB6	Outside wall – balcony	191.4	1.131	216.5	0.633	121.2
TB7	Outside wall – slab	121.4	1.086	131.8	0.051	6.2
TB8	Outside wall (overhang)	42.7	0.321	13.7	0.664	28.4
TB9	Outside wall (no overhang)	19.8	0.320	6.3	0.395	7.8
	Entire building	1077.4	–	667.0	–	213.1

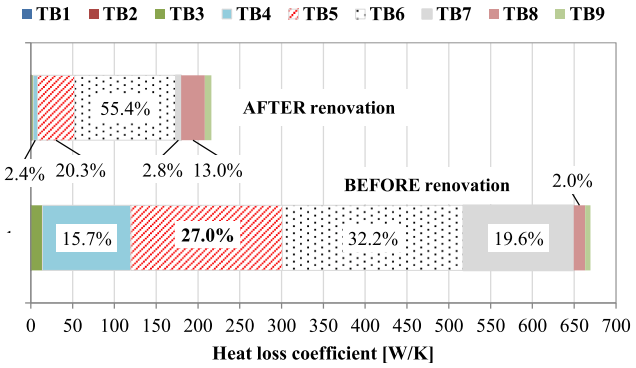

Fig. 10. Contribution of the various thermal bridge typologies to the overall heat losses due to thermal bridges (before and after renovation).

commonly responsible for very high heat losses, especially in case of exposed RC beams and balconies [37,38]. However, despite the lower linear thermal transmittance, TB5 (connection between walls and windows) is also very impacting because of its very high overall length. This makes its contribution to the overall share as high as 27.0%, immediately after TB6 that accounts for 32.2% of the total (see Fig. 10).

Coming now to the renovated building, the proposed solution ensures a significant reduction in the linear thermal transmittance of almost all thermal bridges. For instance, in the connection between walls and balconies (TB6) Ψ_{out} drops from 1.131 W•m^{-1} K^{-1} to 0.633 W•m^{-1} K^{-1} (Table 8): however, this value still keeps quite high, since balconies are a very hard thermal bridge that cannot be fully corrected by just an ETICS insulation strategy [39]. Actually, Ilomets et al. showed that RC balconies in insulated buildings can be responsible of up to 15% of the overall heat losses [40]. In the present study, their contribution to the heat losses is relevant, with a share of 55.4% of the total (see Fig. 10). This means that further improvements to thermal bridges in the pilot building should give priority to the balconies, for instance through their continuous insulation, which however involves non-negligible technical difficulties and implementation costs. Other efficient solutions are available to reduce the heat transfer through balcony slabs: for instance, Ge et al. demonstrated that, by adopting insulated load-bearing thermal brakes, the energy consumption for space heating can be reduced by 5–13% [41]. However, this kind of solution is suitable in new constructions, but its adoption would be very costly and disrupting in case of renovation.

The connection between wall and windows (TB5) is very well corrected. Indeed, Ψ_{out} drops from 0.392 W•m^{-1} K^{-1} to 0.096 W•m^{-1} K^{-1} (Table 8), which is a very good value for this kind of detail [40]: this result is also due to the new position of the window frame, now aligned to the insulating material. Nevertheless, the overall length of this thermal bridge is high, which makes them contribute with the 20.3% to the overall heat losses (Fig. 10).

The proposed renovation solution is also very effective to correct pillars (TB4) and slabs (TB7): their linear thermal transmittance is drastically reduced and almost canceled, which now makes their contribution to the overall heat losses below 3% each (Fig. 10), despite their high length. Finally, the connection between the wall and the roof (TB8 – with overhang, TB9 – without an overhang) shows increased thermal losses after the renovation stage (Table 8): indeed, the combined insulation of walls and roof enhances the conductive heat flux in the RC parapet and the overhang. Their contribution is now almost 17% of the total, suggesting that there is room for improvement, which might for instance involve a continuous insulation of the parapet.

At the building scale, the overall heat loss coefficient for thermal bridges drops from 667.0 W·K^{-1} to 213.1 W·K^{-1}, thus reducing heat losses due to thermal bridges by about 68%.

The reduction of heat losses in the thermal bridges brings also noticeable benefits in terms of mould growth and surface condensation risks, thanks to the higher indoor surface temperatures achieved as reported in Fig. 11. Here, the minimum indoor surface temperatures in each thermal bridge before and after the renovation stage are compared with the condensation and mould growth threshold temperatures. As it is possible to observe, mould growth is avoided for all thermal bridges under study after renovation, thanks to the increased thermal resistance provided by e-CLT and e-PANEL. On the other hand, in the current building state no superficial condensation occurs, while mould growth is predicted for TB1 and TB2 (protruding corner), TB5 (wall-window), TB8 (wall connection with parapet and overhang) and TB9 (wall connection with parapet and without overhang). However, further investigations through transient hygrothermal simulations will assess potential

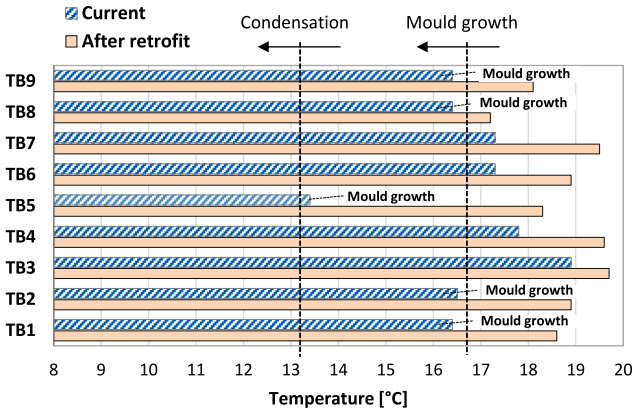

Fig. 11. Minimum indoor surface temperature resulting from the finite element analysis in each thermal bridge, compared with condensation limit (13.2 °C) and mould growth limit (16.7 °C).

interstitial condensation issues in the insulation layer material.

Further finite element analyses were then performed including the metal dampers that connect the e-CLT to the beams, which can be found in thermal bridges from TB6 to TB9. The results suggest that, even if the metal dampers locally increase heat losses, their impact on the overall heat losses due to thermal bridges can be neglected. Indeed, since they only recur in the e-CLT (not in the e-PANEL) and occupy only 25% of the entire beam length in the building, including them would increase the overall heat loss coefficient associated to thermal bridges from 213.1 $W{\cdot}K^{-1}$ to 216.9 $W{\cdot}K^{-1}$ (i.e. by 1.7%), but the impact on the overall heat balance of the renovated building would be even less. In the author's opinion, this does not justify the effort of performing a very detailed finite element analysis of this component.

3.3. Overall heat loss coefficient

The application of the e-PANELs and e-CLTs, along with the insulation of the roof and the replacement of the windows, dramatically lower the magnitude of heat losses if compared to the current state of the building, as demonstrated by the overall heat loss coefficient H′ reported in Table 9. Here, it is possible to appreciate how the coefficient drops down from H' = 1.746 W m^{-2} K^{-1} in the current state to H' = 0.594 W m^{-2} K^{-1} after renovation: this value complies with the Italian regulation concerning major renovations in climate zone B, which requires H' < 0.63 W m^{-2} K^{-1} [28]. In case of low thermal insulation (i.e. with 2 cm less insulating material in the walls), the overall heat loss coefficient H′ would not comply with this regulation; hence, this scenario cannot be acceptable and is not further investigated following.

However, the weight of the thermal bridges in the overall heat balance of the building does not change significantly, as shown in Fig. 12, where a reduction from 21.9% to 20.6% is observed. In general, the percentage distribution has only minor variations, with the floor slab (i.e. the only uninsulated building envelope component) that contributes with a larger share after renovation (around 9.5% of the total), and the roof and the boxes of the window having lower impact.

The results of the energy simulations are summarized in Fig. 13 for the different scenarios introduced in Section 3.1. The plot differentiates the ground, intermediate and top floors, and includes the floor-averaged energy figures of the entire building. The plotted results also account for the contribution of thermal bridges, according to the approach outlined in Section 2.4.

What first emerges is that, in the current building (solid blue hash), the top floor shows the highest energy demand for both space heating (41.5 kWh•m^{-2}, Fig. 13a) and space cooling (27 kWh•m^{-2}, Fig. 13b). This mainly stems from a higher dispersing surface compared to the other floors; furthermore, the roof has an intense longwave radiant heat exchange with the sky vault in the heating season, while also receiving very high solar irradiation in the cooling season. Instead, at the ground floor, the slab is mainly subject to conductive heat transfer with the unheated underground space, whose temperature is constantly closer to the indoor temperature than outdoor air. For this reason, the ground floor is favored in the summer, when it shows the lowest cooling demand (15 kWh•m^{-2}), while in the heating season its energy demand (38.3 kWh•m^{-2}) is higher than in the intermediate floor (Fig. 13a).

By looking at the various retrofit interventions, a drastic reduction in the heating energy demand is expected under both scenario I (basic insulation of external walls) and scenario II (enhanced insulation of external walls), ranging from 37% in the top floor to 76% in the intermediate floor. Instead, no appreciable differences emerge between the two scenarios, thus discouraging the addition of further insulation to the basic thickness. In the cooling season, the benefit of wall insulation is less evident (Fig. 13b), and energy savings are predicted in a range of 4% (top floor) to 33% (ground floor); once again, there is no meaningful difference between basic (scenario I) and enhanced wall insulation (scenario II), and both solutions ensure an average cooling energy reduction by 16.5%.

On the one hand, roof insulation (scenario III, dashed grey hatch) is also a key intervention, since it further reduces the average energy demand of the building by an additional 6.4% in the heating season and 8.7% in the cooling season. Of course, this effect almost entirely pertains to the top floor, while the other floors do not benefit from roof insulation. On the other hand, adding thermal insulation also to the ground slab (scenario IV, mixed hatch) would provide negligible benefits in the heating season at the building scale, and even a slight increase in the average cooling demand. For this reason, and due to the demanding technical and financial effort needed to apply thermal insulation to the ground slab, scenario III is the optimum solution and will be implemented in the pilot building renovation.

It is interesting to observe that the results of the energy simulations discussed so far significantly change if thermal bridges are ignored, which is often the case in dynamic energy simulations: more specifically, neglecting thermal bridges induces an underestimation of space heating and cooling needs As it is possible to see Table 10, the highest deviations occur for space heating under the current building configuration: in this case, an underestimation of around 23% is reported for the entire building. Looking at all the retrofit scenarios, the impact of neglecting thermal bridges in the energy simulations ranges between 15.5% (scenario I and scenario II) and 21.8% (scenario IV). The highest discrepancy occurs in the intermediate floors. Instead, these underestimations are lower when considering cooling energy demand: in fact, the highest deviation is achieved by the current building configuration and amounts to around 12% on average, whereas neglecting thermal bridges in all retrofit scenarios would imply a variation of less than 5%.

These results confirm other data available in the literature. For instance, some studies demonstrated that in multi-story residential buildings with pour-in-place concrete construction located in very cold climates, thermal bridges increase the annual space heating energy demand by up to 40% [42]. In low-rise residential buildings in Italy with RC frames and lightweight hollow brick walls, correcting thermal bridges in the design stage can reduce by 25% the heating demand and by 3% the cooling demand, respectively [39].

Table 9
Overall heat loss coefficient per unit surface (H′).

	Apartment	Before renovation	After renovation	Variation
Ground floor	West side	1.425 W•m^{-2} K^{-1}	0.584 W•m^{-2} K^{-1}	−59.0%
	East side	1.368 W•m^{-2} K^{-1}	0.569 W•m^{-2} K^{-1}	−58.4%
Intermediate floor	West side	2.051 W•m^{-2} K^{-1}	0.665 W•m^{-2} K^{-1}	−67.5%
	East side	2.051 W•m^{-2} K^{-1}	0.665 W•m^{-2} K^{-1}	−67.5%
Top floor	West side	1.633 W•m^{-2} K^{-1}	0.505 W•m^{-2} K^{-1}	−69.0%
	East side	1.633 W•m^{-2} K^{-1}	0.505 W•m^{-2} K^{-1}	−69.0%
Entire building	–	1.746 W•m^{-2} K^{-1}	0.594 W•m^{-2} K^{-1}	−65.9%

4. Conclusions and recommendations

This paper describes the expected hygrothermal and energy performance of a novel technology developed within the ongoing H2020 project e-SAFE, aimed at the combined energy and seismic renovation of RC framed buildings. The proposed retrofit solution makes use of a prefabricated timber-based shell that couples structural CLT-based panels, attached to the existing bearing RC structure through innovative friction dampers, and non-structural wooden framed panels, called e-PANELs, hosting highly efficient windows eventually equipped with shading devices. This new shell is attached to the existing outer walls, thus removing the need to carry out any demolition work and

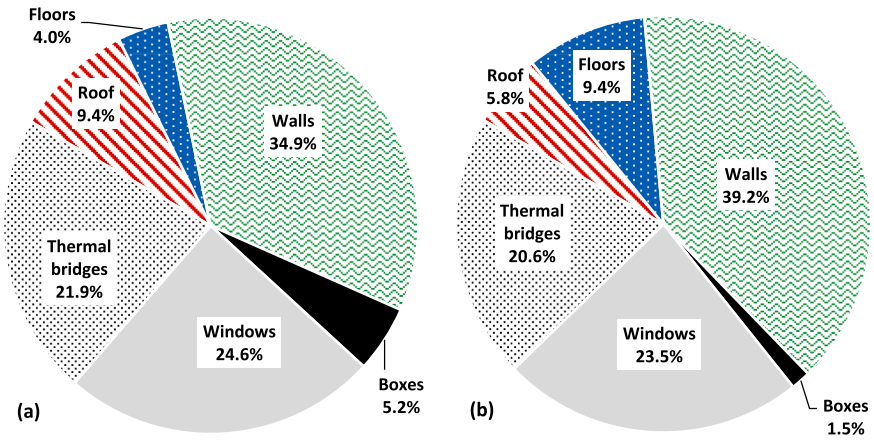

Fig. 12. Percentage distribution of the transmission heat losses in the building: (a) current state, (b) after renovation.

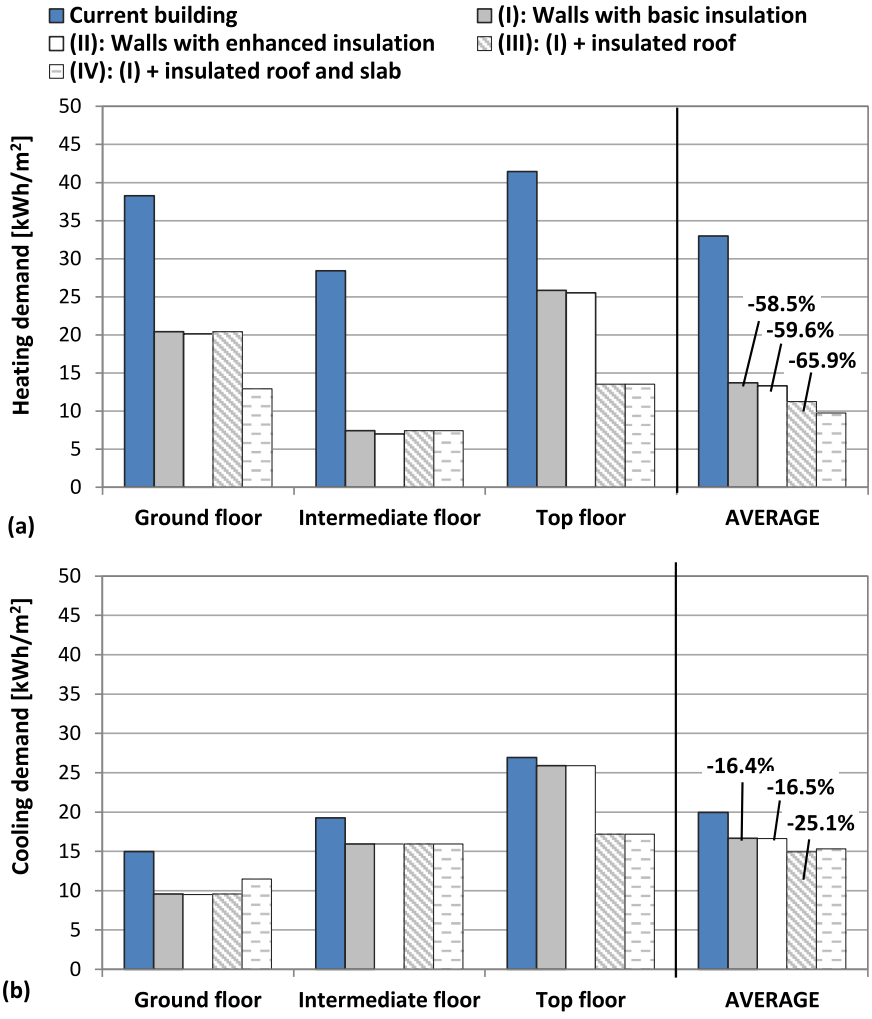

Fig. 13. Results of the dynamic energy simulations, including thermal bridges. (a) Heating demand; (b) Cooling demand.

significantly reducing implementation times and costs, as well as occupants' disruption.

Detailed numerical analyses have been carried out for a pilot building located in Catania (Southern Italy), an old and poorly maintained public housing premise with high heat losses ($U = 1.00$ W•m^{-2} K^{-1} and $U = 5.90$ W•m^{-2} K^{-1} for external walls and windows, respectively) that will be refurbished according to the e-SAFE scheme in 2023. The results of these analyses first revealed that heat losses are cut by about 66% when the new shell is applied, as demonstrated by the calculation of the overall heat transfer coefficient of the entire building that drops from 1.746 W•m^{-2} K^{-1} to 0.594 W•m^{-2} K^{-1}. This entails also significant energy savings in both the heating and cooling seasons: in

Table 10
Percent underestimation of the heating/cooling demand induced by neglecting thermal bridges in dynamic simulations.

Heating demand	Ground floor	Intermediate floor	Top floor	Average
Current building	21.9%	24.2%	19.8%	22.6%
(I): Walls with basic insulation	10.1%	21.8%	14.3%	15.5%
(II): Walls with enhanced insulation	10.3%	22.3%	14.5%	15.7%
(III): (I) + insulated roof	10.1%	21.8%	26.9%	18.8%
(IV): (I) + insulated roof and slab	15.8%	21.8%	26.9%	21.8%
Cooling demand	**Ground floor**	**Intermediate floor**	**Top floor**	**Average**
Current building	19.2%	11.7%	9.6%	12.2%
(I): Walls with basic insulation	7.4%	3.9%	4.3%	4.4%
(II): Walls with enhanced insulation	7.5%	3.9%	4.3%	4.4%
(III): (I) + insulated roof	7.4%	3.9%	6.7%	5.0%
(IV): (I) + insulated roof and slab	6.0%	3.9%	6.7%	4.9%

fact, the heating and cooling energy demands are reduced by around 60% and 16%, in order. Moreover, thermal bridges are considered in detail trough finite element analyses: thanks to the application of continuous insulation from the outside, most of the thermal bridges found in the pilot building are corrected, and the related heat losses reduced from 667 $W{\cdot}K^{-1}$ to 213.1 $W{\cdot}K^{-1}$. This improvement also avoids any mould and surface condensation risks during the coldest months of the year. However, even after retrofit the contribution of thermal bridges to the heat balance is still remarkable: indeed, some thermal bridges – such as the connection of the balconies with the external walls and the connection of the windows with the external walls – cannot be easily corrected through a standard outer insulation of the envelope. In this case, more complex and expensive technological solutions should be introduced to further reduce their linear transmittance values, but a cost-benefit analysis should justify their adoption.

Another interesting finding concerns the influence of thermal bridges in determining the heating and cooling energy savings of the building after the renovation, which may be underestimated by 16% and 5% respectively if thermal bridges are not properly accounted for.

The paper also proposes a novel methodological approach that allows adding the effect of thermal bridges in the post-processing stage of a dynamic simulation, thus avoiding complex and frequently inaccurate inclusion of thermal bridges in the pre-processing stage. The proposed approach is rigorous only in case of simulations with thermostatic control, meaning that at each time step the indoor air temperature is known since it is imposed according to a well-defined schedule, and the required output is the heating/cooling energy needed to counterbalance heat losses and gains. On the other hand, in free-running conditions this approach would not be rigorous: further investigations are needed to measure its reliability.

Finally, the results also suggest that including a detailed numerical analysis of the metal dampers – used to attach the e-CLT to the beams – would increase the overall heat losses associated to thermal bridges by only 1.7%, and even less the overall heating/cooling needs of the renovated building, thus making them negligible for the sake of a quicker and less time-consuming modeling.

The interest of these findings also relies in the fact that the selected pilot is a representative example of residential housing built between 1950s and 1980s in Italy and other Southern European countries, based on an RC frame and lightweight concrete or clay brick walls. The outcomes can thus extend to a significant portion of the European building stock, clarifying the potential effectiveness of the e-SAFE solutions on a large share of buildings, as well possible technical issues that have still to be addressed.

Based on these outcomes, future activities will involve the analysis of colder climate conditions, actual walls' construction features and thermal bridges configurations to fine-tune the envelope technological solutions and scale up the applicability of the e-SAFE scheme to the wider European context.

CRediT authorship contribution statement

Gianpiero Evola: Writing – original draft, Supervision, Methodology, Conceptualization. **Vincenzo Costanzo:** Writing – original draft, Investigation, Data curation. **Alessandra Urso:** Visualization, Software, Investigation. **Carola Tardo:** Writing – original draft, Visualization, Software, Data curation. **Giuseppe Margani:** Writing – review & editing, Supervision, Resources, Funding acquisition.

Declaration of competing interest

The authors declare the following financial interests/personal relationships which may be considered as potential competing interests: Giuseppe Margani reports financial support was provided by Horizon 2020.

Data availability

Data will be made available on request.

Acknowledgments

This paper was carried out in the framework of the "Energy and seismic affordable renovation solutions" (e-SAFE) project, which has received funding from the European Union's Horizon 2020 research and innovation programme under grant agreement No. 893135. Neither the Executive Agency for Small-and-Medium-sized Enterprises (EASME) nor the European Commission is in any way responsible for any use that may be made of the information it contains.

Nomenclature

Symbol Parameter Unit

A	Surface area m^2
A_L	Effective leakage area cm^2
A_{out}	Surface area per unit length (measured on the outer side) m^2/m
c	Specific heat J/(kg•K)
C_S	Stack coefficient $(L/s)^2/(cm^4{\bullet}K)$
C_W	Wind coefficient $(L/s)^2/(cm^4{\bullet}m^2/s^2)$
g	g-value of the glazed surface
H_{TB}	Heat loss coefficient for thermal bridges W/K
H'	Overall heat loss coefficient $W/(m^2{\bullet}K)$
L	Length (of a thermal bridge) M
L_{2D}	Thermal coupling coefficient W/(m•K)
n	Air change rate 1/h
n_{50}	Air change rate under 50 Pa 1/h
p	Pressure Pa
Q_{inf}	Air infiltration rate m^3/s
Q_{TB}	Heat flux through the thermal bridges W
Q_{TOT}	Heat flux per unit length W/(m•K)
R	Thermal resistance $m^2{\bullet}K/W$
RH	Relative humidity %
s	Thickness mm
T_{in}	Indoor air temperature °C
T_{out}	Outdoor air temperature °C
U	Thermal transmittance $W/(m^2{\bullet}K)$

V	Net volume m^3
W	Wind velocity m/s
ε	Thermal emissivity
λ	Thermal conductivity W/(m•K)
ρ	Density kg/m^3
ψ	Linear thermal transmittance W/(m•K)

References

[1] N. Sajn, Energy Efficiency of Buildings: A Nearly Zero-Energy Future? European Parliamentary Research Service, 2016, 476 European Union.

[2] European Commission, Department: Energy. In Focus: Energy Efficiency in Buildings, Brussels, 17 February 2020. Available online: https://ec.europa.eu/info/news/focus-energy-efficiency-buildings-2020-lut-17_en.

[3] G. Margani, Energy and Seismic Renovation Strategies for Sustainable Cities, MDPI, Basel, Switzerland, 2019, ISBN 978-3-03897-945-6.

[4] Presidency of the Council of Ministers Italian Civil Protection Department. National Risk Assessment. Overview of the Potential Major Disasters in Italy.

[5] European Commission, Technology Options for Earthquake Resistant, Eco-Efficient Buildings in Europe: Research Needs, Publications Office of the European Union, Luxembourg, 2014, ISBN 978-92-79-35424-3.

[6] A. Ferrante, G. Mochi, G. Predari, L. Badini, A. Fotopoulou, R. Gulli, G. Semprini, A European project for safer and energy efficient buildings: pro-GET-onE (proactive synergy of integrated efficient technologies on buildings' envelopes), Sustainability 10 (3) (2018) 812.

[7] A. Marini, C. Passoni, A. Belleri, F. Feroldi, M. Preti, G. Metelli, P. Riva, E. Giuriani, G. Plizzari, Combining seismic retrofit with energy refurbishment for the sustainable renovation of RC buildings: a proof of concept, Eur. J. Environ. Civ. Eng. 21 (2017) 1–21.

[8] S. D'Urso, B. Cicero, From the efficiency of nature to parametric design. A holistic approach for sustainable building renovation in seismic regions, Sustainability 11 (2019) 1227.

[9] Ecosism, Geniale cappotto sismico, Available online: http://www.ecosism.com/moduli/geniale/.

[10] A. Artino, G. Evola, G. Margani, Seismic and energy retrofit of apartment buildings through autoclaved aerated concrete (AAC) blocks infill walls, Sustainability 11 (2019) 3939.

[11] D.A. Pohoryles, D.A. Bournas, iRESIST+ Innovative Seismic and Energy Retrofitting of the Existing Building Stock; EUR 30583 EN, Publications Office of the European Union, Luxembourg, 2018.

[12] World Green Building Council, Technical Report Bringing Embodied Carbon Upfront, World Green Building Council, London, UK, 2019.

[13] M. Stepinac, I. Sustersic, I. Gavric, V. Rajcic, Seismic design of timber buildings: highlighted challenges and future trends, Appl. Sci. 10 (2020) 1380.

[14] G. Margani, G. Evola, C. Tardo, E.M. Marino, Energy, seismic, and architectural renovation of RC framed buildings with prefabricated timber panels, Sustainability 12 (12) (2020) 4845.

[15] e-SAFE, (Energy and Seismic AFfordable rEnovation solutions) project. https://esafe-buildings.eu/en/.

[16] F. Boggian, C. Tardo, A. Aloisio, E.M. Marino, R. Tomasi, Experimental cyclic response of a novel friction connection for seismic retrofitting of RC buildings with CLT panels, J. Struct. Eng. 148 (5) (2022), 04022040.

[17] M. Kottek, J. Grieser, C. Beck, B. Rudolf, F. Rubel, World map of the Köppen-Geiger climate classification updated, Meteorol. Z. 15 (3) (2006) 259–263.

[18] EN ISO 6946:2017, Building Components and Building Elements – Thermal Resistance and Thermal Transmittance – Calculation Methods, European Committee for Standardization, 2017.

[19] UNI 10351:2015, Materiali e prodotti per edilizia - Proprietà termoigrometriche - Procedura per la scelta dei valori di progetto, Ente Nazionale Italiano di Unificazione, 2015.

[20] Technical sheet, De rosa website, Retrieved on, https://www.derosasrl.it/public/schede/28447.pdf. (Accessed 22 November 2021) (in Italian).

[21] UNI 10355:1994, Murature e solai. Valori della resistenza termica e metodo di calcolo, Ente Nazionale Italiano di Unificazione, 1994.

[22] EN ISO 10211:2018, Thermal Bridges in Building Construction. Heat Flows and Surface Temperatures. Detailed Calculations, European Committee for Standardization, 2018.

[23] EN 14683:2017, Thermal Bridges in Building Construction - Linear Thermal Transmittance - Simplified Methods and Default Values. Detailed Calculations, European Committee for Standardization, 2017.

[24] A. Capozzoli, V. Corrado, A. Gorrino, P. Soma, Atlante Nazionale dei Ponti Termici. Conforme alle UNI EN ISO 14683 e UNI EN ISO 10211, Edizioni EDILCLIMA, Novara, Italy, 2011 (in Italian).

[25] EN ISO 13788:2012, Hygrothermal Performance of Building Components and Building Elements – Internal Surface Temperature to Avoid Critical Surface Humidity and Interstitial Condensation – Calculation Methods, European Committee for Standardization, 2012.

[26] IRIS, v.5.0 software, Available from: https://www.anit.it/software-anit/pan/. (Accessed 2 September 2021).

[27] Inter-Ministerial Decree, Adeguamento Linee Guida Nazionali per la Certificazione Energetica Degli Edifici; Allegato 1; Gazzetta Ufficiale della Repubblica Italiana n.162 del 15.7.2015, 26.6.2015. Rome, Italy (in Italian).

[28] Inter-Ministerial Decree, Applicazione delle Metodologie di Calcolo delle Prestazioni Energetiche e Definizione delle Prescrizioni e dei Requisiti Minimi degli Edifici, Ministero dello Sviluppo Economico, 26/06/2015 (in Italian).

[29] US Department of Energy, EnergyPlus version 9.0.1. https://energyplus.net/documentation. (Accessed 7 April 2022).

[30] ASHRAE Handbook – Fundamentals, Chapter 26: Ventilation and Infiltration, S.I. Edition, American Society of Heating, Refrigerating and Air-Conditioning Systems, Atlanta, GA, USA, 2009.

[31] UNI/TS 11300-1:2014, Prestazioni energetiche degli edifici - Parte 1: Determinazione del fabbisogno di energia termica dell'edificio per la climatizzazione estiva ed invernale, Ente Nazionale Italiano di Unificazione, 2014.

[32] V. Costanzo, G. Evola, M. Infantone, L. Marletta, Updated Typical Weather Years for the energy simulation of buildings in Mediterranean climate. A case study for Sicily, Energies 13 (16) (2020) 4115.

[33] D.J. Thevenard, A.P. Brunger, The development of typical weather years for international locations: Part I, algorithms, Build. Eng. 108 (2002) 376–383.

[34] Y.J. Huang, F. Su, D. Sheo, M. Krarti, Development of 3012 IWEC2 weather files for international locations (RP-1477), Build. Eng. 120 (2014) 340–355.

[35] J.R. de Freitas, E.G. da Cunha, Thermal bridges modeling in South Brazil climate: three different approaches, Energy Build. 169 (2018) 271–282.

[36] G. Evola, V. Costanzo, L. Marletta, Hygrothermal and acoustic performance of two innovative envelope renovation solutions developed in the e-SAFE Project, Energies 14 (13) (2021) 4006.

[37] J. Lu, Y. Xue, Z. Wang, Y. Fan, Optimized mitigation of heat loss by avoiding wall-to-floor thermal bridges in reinforced concrete buildings, J. Build. Eng. 30 (2020), 101214.

[38] T. Basiricò, A. Cottone, D. Enea, Analytical mathematical modeling of the thermal bridge between reinforced concrete wall and inter-floor slab, Sustainability 12 (2020) 9964.

[39] G. Evola, G. Margani, L. Marletta, Energy and cost evaluation of thermal bridge correction in Mediterranean climate, Energy Build. 43 (2011) 2385–2393.

[40] S. Ilomets, K. Kuusk, L. Paap, E. Arumägi, T. Kalamees, Impact of linear thermal bridges on thermal transmittance of renovated apartment buildings, J. Civ. Eng. Manag. 23 (1) (2017) 96–104.

[41] H. Ge, V.R. McClung, S. Zhang, Impact of balcony thermal bridges on the overall thermal performance of multi-unit residential buildings: a case study, Energy Build. 60 (2013) 163–173.

[42] H. Ge, F. Baba, Effect of dynamic modeling of thermal bridges on the energy performance of residential buildings with high thermal mass for cold climates, Sustain. Cities Soc. 34 (2017) 250–263.